

Effect of Ga³⁺ and Gd³⁺ ions substitution on the structural and optical properties of Ce³⁺-doped yttrium aluminium garnet phosphor nanopowders

A. H. Wako,^{a*} F. B. Dejene^a and H. C. Swart^b

ABSTRACT: The structural and optical properties of commercially obtained Y₃Al₅O₁₂:Ce³⁺ phosphor were investigated by replacing Al³⁺ with Ga³⁺ and Y³⁺ with Gd³⁺ in the Y₃Al₅O₁₂:Ce³⁺ structure to form Y₃(Al,Ga)₅O₁₂:Ce³⁺ and (Y,Gd)₃Al₅O₁₂:Ce³⁺. X-Ray diffraction (XRD) results showed slight 2-theta peak shifts to lower angles when Ga³⁺ was used and to higher angles when Gd³⁺ was used, with respect to peaks from Y₃Al₅O₁₂:Ce³⁺ and JCPDS card no. 73–1370. This could be attributed to induced crystal-field effects due to the different ionic sizes of Ga³⁺ and Gd³⁺ compared with Al³⁺ and Y³⁺. The photoluminescence (PL) spectra showed broad excitation from 350 to 550 nm with a maximum at 472 nm, and broad emission bands from 500 to 650 nm, centred at 578 nm for Y₃Al₅O₁₂:Ce³⁺ arising from the 5d → 4f transition of Ce³⁺. PL revealed a blue shift for Ga³⁺ substitution and a red shift for Gd³⁺ substitution. UV–Vis showed two absorption peaks at 357 and 457 nm for Y₃Al₅O₁₂:Ce³⁺, with peaks shifting to 432 nm for Ga³⁺ and 460 nm for Gd³⁺ substitutions. Changes in the trap levels or in the depth and number of traps due to Ce³⁺ were analysed using thermoluminescence (TL) spectroscopy. This revealed the existence of shallow and deep traps. It was observed that Ga³⁺ substitution contributes to the shallowest traps at 74 °C and fewer deep traps at 163 °C, followed by Gd³⁺ with shallow traps at 87 °C and deep traps at 146 °C. Copyright © 2016 John Wiley & Sons, Ltd.

Keywords: Y₃(Al,Ga)₅O₁₂:Ce³⁺; (Y,Gd)₃Al₅O₁₂:Ce³⁺ substitution; thermoluminescence; trap depths

Introduction

Extensive research on inorganic luminescent materials with activators showing allowed f–d transitions has gained momentum over the past decade. Lanthanide ions are very sensitive to the chemistry of their environment because the d-states are not shielded. This is important for the manufacture of white light-emitting diodes (LEDs) because the f–d absorption has to be within the UV to blue spectral region. A number of factors may result in alterations in the chemical environment, for example: changes in the charge density of the bond lengths caused by differences in electronegativity between the dopant and its surroundings, leading to changes in covalency; changes in the crystal-field splitting of the 5d state due to differences in the charge of the surrounding ions; or changes in metal–ligand distances (1). An increase in crystal-field splitting and high covalency will shift the f–d transition to lower energies and vice versa.

Yttrium aluminium garnet (Y₃Al₅O₁₂) is one of the most important optical materials and, because of its wide band gap and excellent radiation conversion efficiency, has a wide range of applications in cathode ray tubes (CRTs), field emission displays (FEDs) and scintillators (2). It is also suitable for use as a host material for solid-state phosphors because of its good chemical stability, high quantum yield, low toxicity, low thermal expansion and tuneable emission wavelength (3). Next-generation solid-state lighting is preferred over conventional light sources, such as incandescent and fluorescent lamps, due to its brightness, high radiation efficiency, long life time, compatibility with the environment

(4), low cost, lack of mercury, compactness (5) energy saving and reliability (6).

The conversion of UV/blue radiation into white radiation using a phosphor is one of the most significant technologies in solid-state lighting (7). Upon excitation with blue radiation, cerium-activated Y₃Al₅O₁₂ (Y₃Al₅O₁₂:Ce³⁺) emits a yellow broad band that, when combined with a blue LED, produces white light (6). The yellow emission band ranging from 510 nm to >600 nm originates from the allowed 5d–4f electronic transition of Ce³⁺ to the spin-orbit split ²F_{7/2} and ²F_{5/2} levels (8), which efficiently absorb blue excitation light from 450 to 470 nm to produce white light (4). For general lighting, an ideal white light needs to be generated. Hence, there is a need to obtain a phosphor with a broad emission band covering the green and red regions in the blue-light excitation (5).

One way to achieve this is to modify the composition of the host lattice to obtain phosphors with adjustable wavelengths that match blue LEDs. This can be done by doping the garnet lattice with suitable cations to adjust the emission colour slightly (6), either by expanding the Y₃Al₅O₁₂:Ce³⁺ emission band to induce a red shift (7) or by reducing the Y₃Al₅O₁₂:Ce³⁺ emission band to

* Correspondence to: A. H. Wako, Department of Physics, University of the Free State, QwaQwa Campus, Private Bag X13, Phuthaditjhaba 9866, South Africa. E-mail: alihwako@gmail.com

^a Department of Physics, University of the Free State, Phuthaditjhaba, South Africa

^b Department of Physics, University of the Free State, Bloemfontein, South Africa

give a blue shift. The emission wavelength can be tuned by partially or totally substituting trivalent ions of different sizes into the $Y_3Al_5O_{12}:Ce^{3+}$ lattice matrix. Larger ions will cause lattice expansion, resulting in a red shift, whereas smaller ions will result in a blue shift. This is because by increasing or decreasing the ionic radii in the garnet host lattice, the cubic symmetry around the rare earth ions becomes distorted (3).

In this work, we report changes in the structure and emission wavelength of a commercial $Y_3Al_5O_{12}:Ce^{3+}$ phosphor when Y^{3+} was replaced with Gd^{3+} to obtain $(Y,Gd)_3Al_5O_{12}:Ce^{3+}$ and Al^{3+} was replaced with Ga^{3+} to obtain $Y_3(Al,Ga)_5O_{12}:Ce^{3+}$, respectively, vis-à-vis variation of the crystal-field energy levels of Ce^{3+} .

Experimental

Commercial $Y_3Al_5O_{12}:Ce^{3+}$, $Y_3(Al,Ga)_5O_{12}:Ce^{3+}$ and $(Y,Gd)_3Al_5O_{12}:Ce^{3+}$ phosphor powders were obtained from Phosphor Technology (Stevenage, Herts). The structural and phase compositions were determined using a Bruker-AXS D8 Advance X-ray diffractometer (Bruker Corp., Karlsruhe, Germany) operating at 40 kV and 4 mA, using $CuK\alpha = 0.15406$ nm from 15° to 65° (2θ), with a scan rate of 0.39° (2θ)/min and step scans of 0.02° (2θ). (UV) Absorption/reflectance characteristics were measured over the range 250–700 nm using a Perkin-Elmer Scan Lambda 950 UV-Vis spectrophotometer (Rodgau, Germany) with a 319.20 nm excitation lamp and 860.80 nm monochromator with a band pass slit width of 2.0 nm, a scan speed of 141.20 nm/min and a data interval of 0.5 nm. Photoluminescence (PL) excitation and emission spectra were measured at room temperature using a Cary Eclipse luminescence spectrometer (model LS-55) (Santa Clara, CA) with a built-in 150 W xenon flash lamp as the excitation source and a grating to select a suitable excitation wavelength with excitation and emission slit widths of 2.5 nm, a scan rate of 600 nm/min, a medium photomultiplier tube voltage, an excitation filter of 335–620 nm and an emission filter of 550–1100 nm. Thermoluminescence (TL) analysis was carried out above room temperature using a Nucleonix 1009I TL reader to investigate traps and defects in the band gap of the

phosphors. The samples were excited with UV radiation and heating from room temperature to $400^\circ C$ at a constant heating rate of $1^\circ C/s$ under thermal stimulation.

Results and discussions

Structure and XRD analysis

$Y_3Al_5O_{12}$ has a cubic garnet-type structure commonly represented in a general form as $\{A\}_3\{C\}_2\{D\}_3(O)_{12}$. It has a *bcc* structure of space group *I* $a-3d$ (230) with 160 atoms in the cubic (primitive) cell and the following cell parameters: $a = 12.01$ Å; cell ratio, $a/b = 1.0$, $b/c = 1.0$, $c/a = 1.0$; and cell volume = 1732.32 Å³.

The $\{A\}$ -cations are eight-coordinated to eight O in dodecahedra and occupy the 24(c) sites. Al occupies two different sites; the Al $\{C\}$ -cations are octahedrally bonded occupying the 16(a) sites and the Al $\{D\}$ -cations are tetrahedrally bonded occupying the 24 (d) sites (8). The O atoms occupy the 96(h) sites and their specific positions within the unit cell vary for different garnets (9).

The XRD patterns of the $Y_3Al_5O_{12}:Ce^{3+}$, $Y_3(Al,Ga)_5O_{12}:Ce^{3+}$ and $(Y,Gd)_3Al_5O_{12}:Ce^{3+}$ phosphor powders are shown in Fig. 1. It can be seen that the diffraction peaks are shifted slightly to the lower 2θ angles for $Y_3(Al,Ga)_5O_{12}:Ce^{3+}$ and to higher 2θ angles for $(Y,Gd)_3Al_5O_{12}:Ce^{3+}$. This is also depicted in Fig. 2(c). It is well known that the size of the ionic radius of the substituting cation influences the resultant change in the lattice parameters. This can be attributed to the change in the host lattice caused by the larger ionic size of Ga^{3+} (0.062 nm) compared with that of Al^{3+} (0.053 nm), which causes an increase in the d-spacing, as confirmed in Fig. 2(a). Hence, there is an XRD peak shift towards lower angles (10). On the same note, because the ionic size of Gd^{3+} (0.1053 nm) (11) is greater than that of Y^{3+} (0.102 nm) (12), substituting Gd^{3+} also results in lattice expansion causing an XRD peak shift to lower angles.

It is worth noting that, with reference to $Y_3Al_5O_{12}:Ce^{3+}$, the shift is -0.39° for Ga^{3+} and -0.1° for Gd^{3+} . So Ga^{3+} shifts slightly towards lower angles and Gd^{3+} shifts slightly towards the higher angles compared with $Y_3(Al,Ga)_5O_{12}:Ce^{3+}$. This is due to the resultant difference in the radii after substitution, which is smaller between

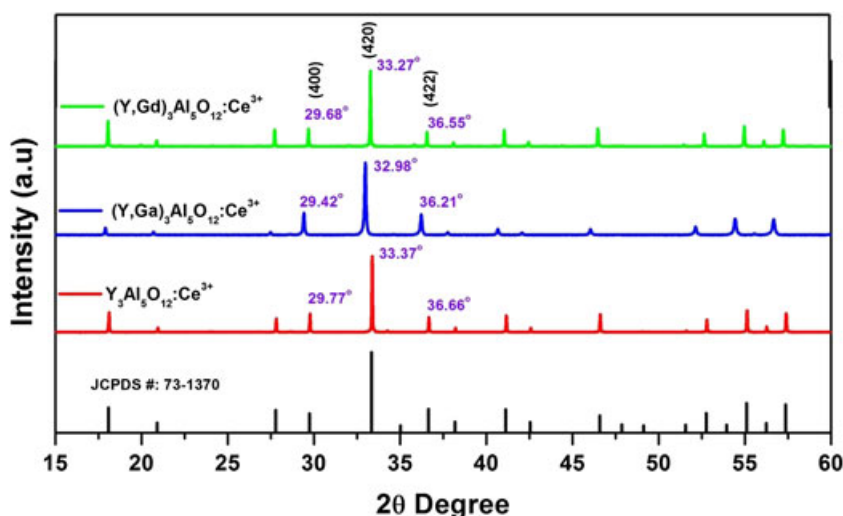


Figure 1. XRD patterns of the $Y_3Al_5O_{12}:Ce^{3+}$, $Y_3(Al,Ga)_5O_{12}:Ce^{3+}$ and $(Y,Gd)_3Al_5O_{12}:Ce^{3+}$.

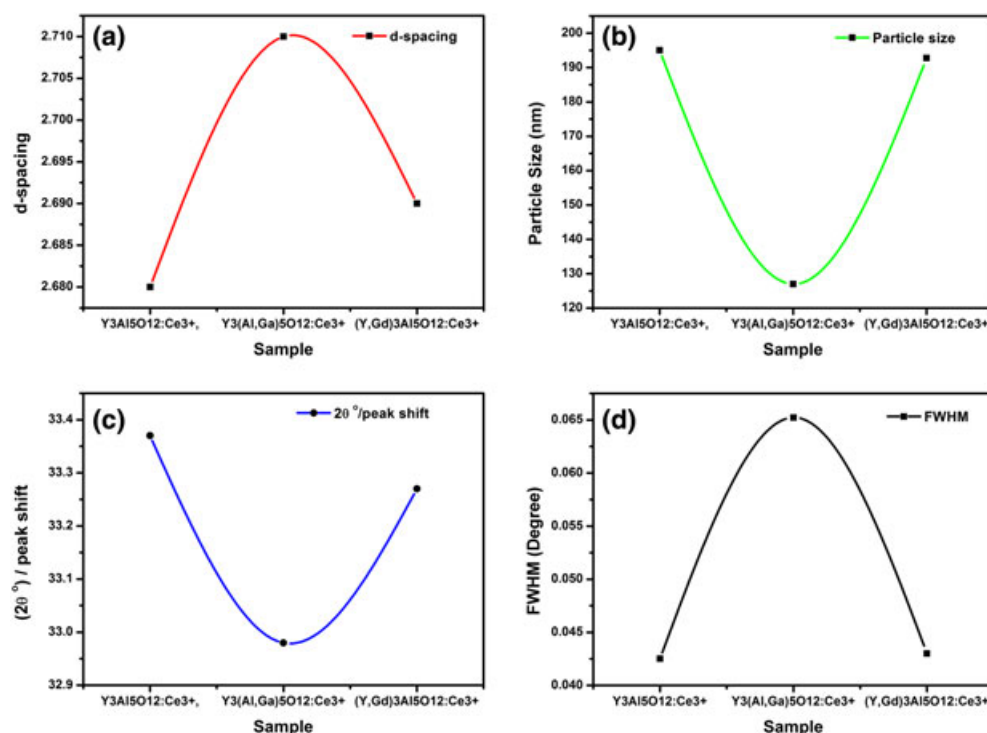


Figure 2. The effect of Ga³⁺/Gd³⁺ ion substitution in to the Y₃Al₅O₁₂:Ce³⁺ composition on the (a) d-spacing, (b) particle size, (c) 2-theta peak shift, and (d) FWHM.

Gd³⁺ and Y³⁺ (0.003 nm) and larger between Ga³⁺ and Al³⁺ (0.009 nm).

The average crystallite sizes calculated for the (420) direction were obtained using Scherrer's equation:

$$D = \frac{K\lambda}{\beta \cos \theta} \quad (1)$$

and are shown in Fig. 2(b), where D is the mean particle size, K is a geometric factor, λ is the X-ray wavelength and β is the full-width at half maximum (FWHM). It can be observed that particle size decreased with Ga³⁺ substitution, resulting in a blue shift in the PL spectra (Fig. 3a,b) (13), and increased with Gd³⁺ substitution, which induced a red shift in the PL spectra. Figure 2(d) shows this variation in the FWHM on addition of Ga³⁺ and Gd³⁺ ions into the Y₃Al₅O₁₂:Ce³⁺ structure, which is larger for Ga³⁺ and narrower for Gd³⁺ substitution.

Photoluminescence

Figure 3(a) shows the normalized room temperature PL excitation spectra at emission wavelengths of 568, 578 and 588 nm, whereas Fig. 3(b) shows emission spectra at excitation wavelengths of 438, 462 and 467 nm for Y₃Al₅O₁₂:Ce³⁺, Y₃(Al,Ga)₅O₁₂:Ce³⁺ and (Y,Gd)₃Al₅O₁₂:Ce³⁺ powders, respectively, as recorded using a Cary Eclipse PL spectrometer.

The broad band excitation at 400–525 nm is due to electronic transition from the 4f ground state to the crystal-field split 5d states of the Ce³⁺ ion. Blue excitation raises the electron in the Ce³⁺ ion from the 4f ground state to the 5d level, which is then be transferred to the lower 2D(5d) excited state (6). Green–yellow emission emanates from within the cubic Y₃Al₅O₁₂ lattice due to electronic transitions from the 5d excited states to the split 4f (²F_{7/2} and ²F_{5/2}) ground states characteristic of Ce³⁺ ions (4).

Electrons excited to the 5d level of Ce³⁺ ions decay non-radiatively to the 4f levels of Ce³⁺ ions (14), resulting in broad emission bands centred at 568, 578 and 588 nm for Y₃Al₅O₁₂:Ce³⁺, Y₃(Al,Ga)₅O₁₂:Ce³⁺ and (Y,Gd)₃Al₅O₁₂:Ce³⁺ powders, respectively. The emission from Ce³⁺ is very sensitive to and is affected by changes in the local lattice structure due to the resultant crystal field effects. Hence, the peak position of the emission depends on the environment of the garnet host, which may bring about a blue, or red, shift in the Ce³⁺ emission when co-activated with Ga³⁺ or Gd³⁺. Aluminate garnets are relatively flexible in substituting Y³⁺ ions in the dodecahedral sites and Al³⁺ in the tetrahedral/octahedral sites, which makes it is easy to modify the host Y₃Al₅O₁₂ composition in order to alter the Ce³⁺ emission band to meet spectral requirements (5).

When Gd³⁺ (or La³⁺) was used to substitute for the Y³⁺ site in the Y₃Al₅O₁₂ lattice, the emission peak of the phosphor powder shifted to a longer wavelength (15). Replacement of Y³⁺ with Gd³⁺ shifted the emission peak towards a longer wavelength (588 nm) relative to the 578 nm emission peak from Y₃Al₅O₁₂:Ce³⁺, as shown in Fig. 3(b). Such a shift is mainly due to changes in the lowest 5d¹ crystal-field energy level, which is strongly affected by the local electrostatic field determined by the crystalline structure of the YAG lattice. The lowest/first excited state of Ce³⁺ originates from the 5d configuration. Because Y³⁺ occupies a dodecahedral site in Y₃Al₅O₁₂ that has a tetragonal symmetry and because of the symmetry or the crystal field exerted by the host ligand ions and spin-orbit interaction, the 5d state degenerates into five levels resulting in five absorption bands, 460, 340, 261, 224 and 205 nm. Of these, the absorption bands at 460 and 340 nm are commonly observed at room temperature, as shown in the absorption spectra of Fig. 4.

Because the ionic size of Gd³⁺ is greater than that of Y³⁺, replacing Y³⁺ with Gd³⁺ causes lattice expansion leading to an increase in the crystal-field interaction of Ce³⁺ (7). As the crystal-field splitting of the 5d energy levels of the Ce³⁺ ion increases and the

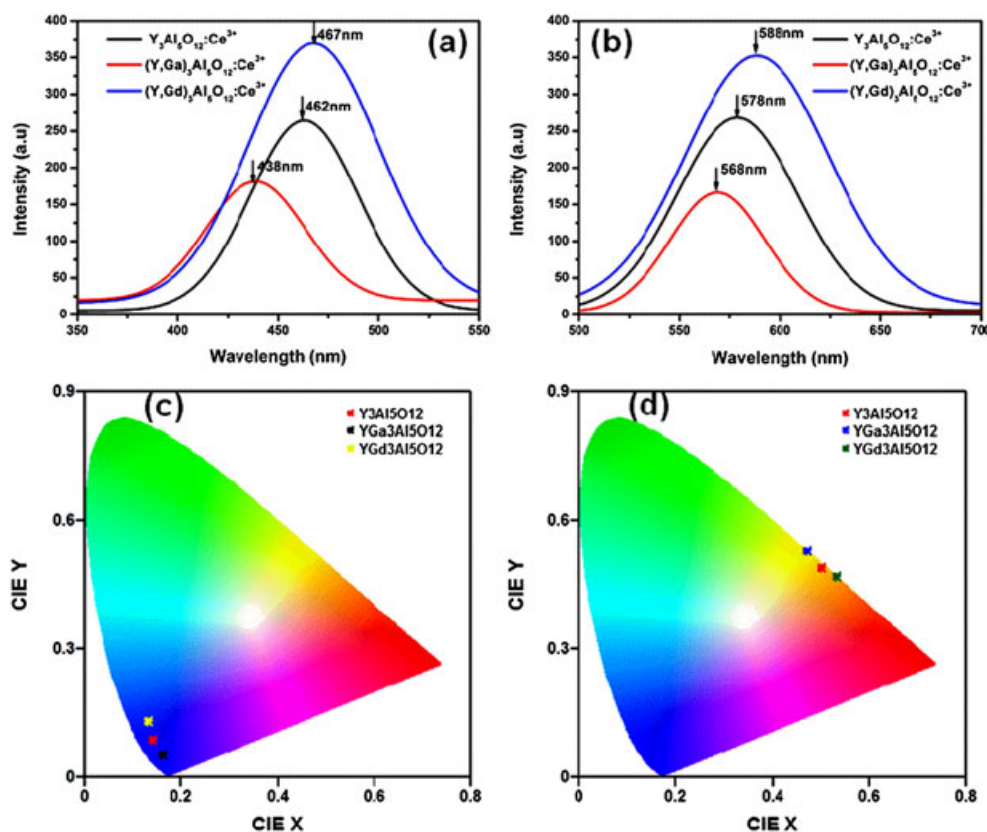


Figure 3. (a) Excitation and (b) emission spectra, and (c, d) chromaticity diagram depicting CIE colour co-ordinates for the $\text{Y}_3\text{Al}_5\text{O}_{12}:\text{Ce}^{3+}$, $\text{Y}_3(\text{Al,Ga})_5\text{O}_{12}:\text{Ce}^{3+}$ and $(\text{Y,Gd})_3\text{Al}_5\text{O}_{12}:\text{Ce}^{3+}$ powders, respectively.

energy difference between the lowest 5d sublevel and the ground state of the 4f configuration of Ce^{3+} becomes smaller, the emission band shifts to a longer wavelength (red shift). In other words, more splitting down-shifts the lowest excited 5d states of Ce^{3+} to lower energies leading to the emission of light of longer wavelengths.

It is well known that the ionic radius decreases and electronegativity (χ) increases with atomic number. In the ionic relationship, Me/Re–O–Ce (Me/Re = Gd subs Y), the electronegativity (χ) of Gd^{3+} (1.20) is smaller than that of Y^{3+} (1.22), and the ionicity of the Me/Re–O band decreases with additional Gd^{3+} content. This induces an increase in the ionicity of O–Ce in Lu–O–Ce and a red shift in the emission occurs (15). The increase in ionicity brings the 5d energy level of the Ce^{3+} ion closer to the 4f ground state, which shifts the emission to higher wavelengths; this is consistent with the observed emission properties shown in Fig. 3. The magnitude of the crystal-field splitting is mainly affected by the Ce–O bond length (lattice constant), the molecular orbital overlap between Ce^{3+} and O^{2-} , and the electronegativity (χ) value. The dependence of crystal-field splitting D_q on the (bond length) lattice constant can be shown using the equation:

$$D_q = \frac{Ze^2r^4}{6R^5} \quad (2)$$

where Z is the charge of the anion ($Z = 2$ for O^{2-}), e is the charge of an electron, r is the radius of the d wave function and R is the bond length (11). Therefore, when the Ce^{3+} – O^{2-} bond length (lattice constant) become shorter, the magnitude of the crystal-field strength is increased and, because crystal-field splitting D_q is proportional to $1/R^5$, it lowers the 5d band of Ce^{3+} , resulting in a red

shift (5). Hence, compared with $\text{Y}_3\text{Al}_5\text{O}_{12}:\text{Ce}^{3+}$, the spectrum of $(\text{Y,Gd})_3\text{Al}_5\text{O}_{12}:\text{Ce}^{3+}$ is shifted slightly to the red, because of reduced local symmetry (16).

By contrast, substitution of Al^{3+} with Ga^{3+} shifts the emission towards a shorter wavelength (568 nm), as seen in Fig. 3(b), relative to the emission peak at 578 nm for $\text{Y}_3\text{Al}_5\text{O}_{12}:\text{Ce}^{3+}$. It has been reported that substituting a Ga^{3+} ion in the Al^{3+} site induces a blue shift in the emission wavelength (8). In the bond relation, Me–O–Ce (Me = Al-doped Ga), the electronegativity (χ) of Ga (1.81) is larger than that of Al^{3+} (1.61), and the ionicity of Me–O is decreased with the addition of Ga^{3+} content, which enhances the energy gap of O–Ce in Me–O–Ce. Therefore, a blue shift in the emission occurs, which means a higher energy Ce^{3+} 4f–5d absorption due to the increased ionicity of O–Ce (15), as shown in Fig. 4(a) which compares the luminescence properties of $\text{Y}_3\text{Al}_5\text{O}_{12}:\text{Ce}^{3+}$, $\text{Y}_3(\text{Al,Ga})_5\text{O}_{12}:\text{Ce}^{3+}$ and $(\text{Y,Gd})_3\text{Al}_5\text{O}_{12}:\text{Ce}^{3+}$ with respect to variations in the crystal-field energy levels of Ce^{3+} .

Cerium belongs to the lanthanides, with an electronic configuration in the form $[\text{Xe}]4f^n5s^m$. It can exist as an atom or as a free ion. The 6s shell may be empty ($m = 0$), especially in compounds, occupied by one electron ($m = 1$) or occupied by two electrons ($m = 2$). When filled completely, the 4f shell is composed of 14 electrons. The 4fⁿ energy levels are not affected by the host environment because they are completely shielded by the filled 5p⁶ and 5s² shells of the [Xe] configuration. However, an electron in a 5d orbital is not shielded completely and its energy is very susceptible to changes in the crystalline environment.

In $\text{Y}_3\text{Al}_5\text{O}_{12}:\text{Ce}^{3+}$, the ground and excited electronic configurations of the Ce^{3+} ion are 4f¹ and 5d¹ and it has only one electron in the 4f state. The excited 5d¹ level strongly interacts with the host

$Y_3Al_5O_{12}:Ce^{3+}$ structure. The emission wavelength of $(Y,Gd)_3Al_5O_{12}:Ce^{3+}$ is longer, followed by the emission wavelength of $Y_3Al_5O_{12}:Ce^{3+}$ and then $Y_3(Al,Ga)_5O_{12}:Ce^{3+}$ due to a relative decrease in ionicity resulting from the decrease in energy due to electron transfer from O^{2-} to Ce^{3+} (15), as represented in Fig. 4(b). The symmetry of the host matrix and the chemical environment around the Ce^{3+} ions greatly affect these split energy levels and the splitting patterns (18).

The (x,y) coordinates of a Commission International de l'Eclairage (CIE) diagram can be used to describe the colour properties of a light source. The CIE chromaticity of $Y_3Al_5O_{12}:Ce^{3+}$, $Y_3(Al,Ga)_5O_{12}:Ce^{3+}$ and $(Y,Gd)_3Al_5O_{12}:Ce^{3+}$ powders are presented in Fig. 3(c,d) and depict the corresponding excitation and emission peak shifts shown in Fig. 3(a,b). The CIE coordinates shift toward the longer wavelength of the CIE map for Gd^{3+} substitution and to the shorter wavelength for Ga^{3+} substitution. The CIE (x,y) colour coordinates of $Y_3Al_5O_{12}:Ce^{3+}$, $Y_3(Al,Ga)_5O_{12}:Ce^{3+}$ and $(Y,Gd)_3Al_5O_{12}:Ce^{3+}$ are (0.5, 0.49), (0.47, 0.53) and (0.53, 0.47), respectively. To generate white light for indoor illumination, a white LED combines the blue light emitted from the LED chip with the yellowish emission from the phosphor (15). The wavelengths of the blue light (excitation) source are 462, 438 and 467 nm with the chromaticity point located at (0.14, 0.09), (0.16, 0.05) and (0.13, 0.13) for $Y_3Al_5O_{12}:Ce^{3+}$, $Y_3(Al,Ga)_5O_{12}:Ce^{3+}$ and $(Y,Gd)_3Al_5O_{12}:Ce^{3+}$.

UV-Vis analysis

Figure 5(a) shows how absorption is influenced by replacement of Y^{3+} with Gd^{3+} and Al^{3+} with Ga^{3+} in the $Y_3Al_5O_{12}:Ce^{3+}$ garnet structure. The absorption bands of the colour centres were found to be broad and peaked at approximately 457, 432 and 460 nm for $Y_3Al_5O_{12}:Ce^{3+}$, $Y_3(Al,Ga)_5O_{12}:Ce^{3+}$ and $(Y,Gd)_3Al_5O_{12}:Ce^{3+}$ powders, respectively, in the range between 250 and 500 nm. Each spectrum showed two absorption peaks corresponding with the PL excitation wavelengths of each sample, as shown in Fig. 3(a). Also, the main peaks shifted, to a lower absorption wavelength (432 nm) for Ga^{3+} substitutions and a higher wavelength (460 nm) for Gd^{3+} substitutions with respect to 458 nm for $Y_3Al_5O_{12}:Ce^{3+}$. The absorption intensities also varied, being highest for Gd^{3+} and lowest for Ga^{3+} compared with $Y_3Al_5O_{12}:Ce^{3+}$. The optical band gap of $Y_3Al_5O_{12}:Ce^{3+}$ is in the order of 6.6 eV, in which the valence band comprises filled oxygen 2p orbitals, whereas the conduction band consists of yttrium 4d orbitals (17).

The absorption coefficient spectra were obtained by conversion from the reflectance spectra using the Kubelka–Munk function:

$$F(R) = \frac{(1-R)^2}{2R} = \frac{k}{s} = \frac{Ac}{s} \quad (3)$$

where R is the absolute reflectance, k the molar absorption coefficient, s the scattering coefficient, c concentration of the absorbing species and A is the absorbance. This equation is usually applied to materials that have high light scattering and absorbing particles in their structures (19). Equation (2) can be modified by multiplying the $F(R)$ function by $h\nu$:

$$(F(R)*h\nu)^n \quad (4)$$

where h is Planck's constant and n is the value of the type of transition, whereby $n = 1/2$ for a direct allowed transition, $n = 2$ for non-metallic materials, $n = 3/2$ for a direct forbidden transition, $n = 2$ for an indirect allowed transition and $n = 3$ for an indirect forbidden transition.

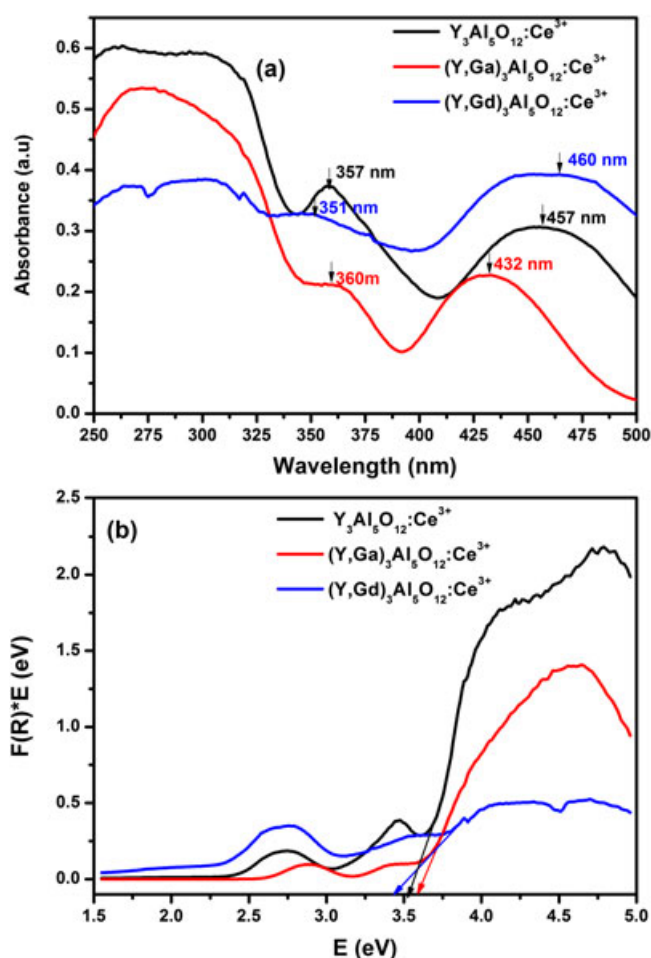


Figure 5. (a) UV-Vis absorption spectra and (b) Tauc's plot for $Y_3Al_5O_{12}:Ce^{3+}$, $Y_3(Al,Ga)_5O_{12}:Ce^{3+}$ and $(Y,Gd)_3Al_5O_{12}:Ce^{3+}$.

The optical band-gap energies (E_g) (eV) were estimated from the intercept of the extrapolated linear portion from the high slope region of the $(F(R) * h\nu)^n$ vs. $h\nu$ plot known as Tauc's plot along the $h\nu$ axis (19), as shown in Fig. 5(b). It can be seen that (E_g) is greatly influenced by the presence of the incorporated substituent ions (Ga^{3+} and Gd^{3+}) in the matrix of the host $Y_3Al_5O_{12}:Ce^{3+}$. $E_g \approx 3.3$, 3.5 and 3.6 eV for $(Y,Gd)_3Al_5O_{12}:Ce^{3+}$, $Y_3Al_5O_{12}:Ce^{3+}$ and $Y_3(Al,Ga)_5O_{12}:Ce^{3+}$, respectively. The band-gap energies are seen to correspond with the energy difference between the lowest 5d level and the ground state of 4f configuration of Ce^{3+} , as represented in the schematic energy diagram in Fig. 4. As the crystal-field splitting of 5d energy levels of the Ce^{3+} ion increases, in the case of $(Y,Gd)_3Al_5O_{12}:Ce^{3+}$, or decreases, in the case of $Y_3(Al,Ga)_5O_{12}:Ce^{3+}$, more or less splitting occurs, respectively, and pushes the lowest excited 5d state of Ce^{3+} toward lower energies.

Thermoluminescence

The TL of the $Y_3Al_5O_{12}:Ce^{3+}$, $Y_3(Al,Ga)_5O_{12}:Ce^{3+}$ and $(Y,Gd)_3Al_5O_{12}:Ce^{3+}$ samples was investigated to understand the nature of traps, trapping levels/energies and de-trapping mechanisms (20), and how these might be affected by substitution of the trivalent cations Ga^{3+} and Gd^{3+} into the host ($Y_3Al_5O_{12}:Ce^{3+}$) lattice. TL is the emission of light from an insulator or a semiconductor following the previous absorption of energy after exposure to a certain radiation (21). Exposure to radiation aims to dislodge electrons and

excite them from impurity levels within the crystal lattice into the conduction band. The electrons are then captured by intentional or unintentional traps within the band gap of the material (22). Upon heating, the trapped electrons relax back to their normal, stable, lower-energy positions, releasing energy in the process (23). The traps are then analysed during TL measurement by heating the sample. During the TL measurements, the samples were exposed to UV radiation for the same period (5 min) and the temperature, T ($^{\circ}C$) was increased linearly at a heating rate (β) of $1^{\circ}C/s$ as a function of time t (s); glow curves of intensity (I) as a function of temperature T ($^{\circ}C$) were recorded as shown in Fig. 6(a). The temperature of the TL peak position represents the trap depth/level, whereas the intensity represents the number of traps within the band gap and the energy corresponding to the glow peak is equal to the trap depth (13).

The glow curves for $Y_3(Al,Ga)_5O_{12}:Ce^3$ and $(Y,Gd)_3Al_5O_{12}:Ce^3$ feature two peaks each; one distinguished a maximum peak temperature (T_m) at $74^{\circ}C$ and a shoulder at $163^{\circ}C$ for $Y_3(Al,Ga)_5O_{12}:Ce^3$ and at $87^{\circ}C$ and $146^{\circ}C$ for $(Y,Gd)_3Al_5O_{12}:Ce^3$, whereas the

glow curve of $Y_3Al_5O_{12}:Ce^3$ features only one peak at $162^{\circ}C$. The three peaks at $146^{\circ}C$ for $(Y,Gd)_3Al_5O_{12}:Ce^3$ and $163^{\circ}C$ for $Y_3(Al,Ga)_5O_{12}:Ce^3$ and $162^{\circ}C$ for $Y_3Al_5O_{12}:Ce^3$ might be equivalent to deeper traps (24) although the first two are of low intensity compared with the last. The low intensity of the phosphor can be attributed to the presence of an insufficient number of shallow traps, whereas a deeper trap density is related to longer decay times. Because the concentration of Ce^{3+} remains constant in all the samples, the observed changes in the peak position and intensity could only be due to the substitution of Ga^{3+} and Gd^{3+} into the host ($Y_3Al_5O_{12}$) lattice.

As shown in Fig. 6(b), the highest TL signal was observed for $(Y,Gd)_3Al_5O_{12}:Ce^3$ with a peak at $87^{\circ}C$, followed by $Y_3Al_5O_{12}:Ce^3$ at $162^{\circ}C$, and the lowest for $Y_3(Al,Ga)_5O_{12}:Ce^3$ at $74^{\circ}C$, suggesting presence of trap levels. It has been explained elsewhere that the trap depth is directly proportional to the glow peak maximum (25), therefore, the trap depth of the samples in descending order is $Y_3Al_5O_{12}$ host $>$ $(Y,Gd)_3Al_5O_{12}$ host $>$ $Y_3(Al,Ga)_5O_{12}$ host. It was also observed from the TL peak measurements that the energy

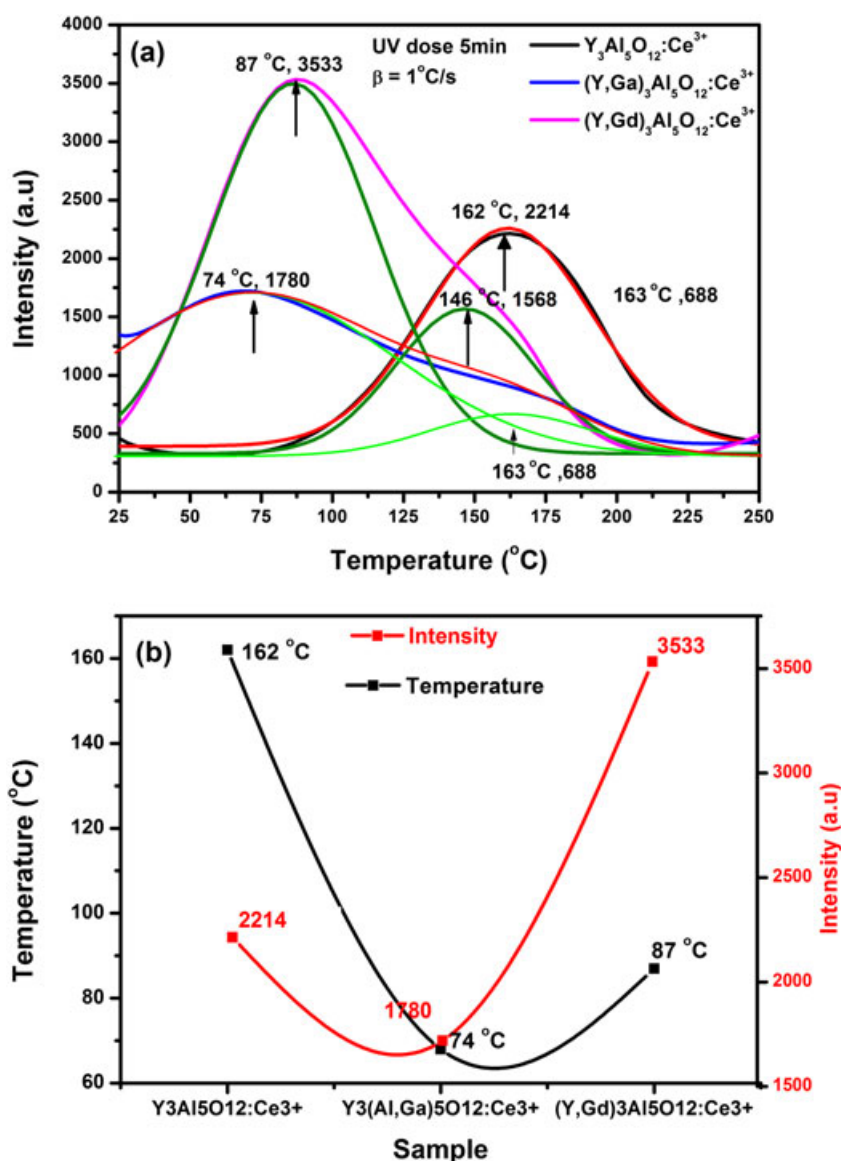


Figure 6. (a) Fitted TL glow curves and (b) peak temperature and intensity curves for the $Y_3Al_5O_{12}:Ce^{3+}$, $Y_3(Al,Ga)_5O_{12}:Ce^{3+}$ and $(Y,Gd)_3Al_5O_{12}:Ce^{3+}$ samples.

traps of trivalent rare earth ions are in the order: $\text{Yb}^{3+} > > \text{Sm}^{3+} > > \text{Dy}^{3+} > \text{Pr}^{3+} > \text{Nd}^{3+} > \text{Er}^{3+} > \text{Ce}^{3+} > \text{Gd}^{3+} > \text{La}^{3+}$ (26), which is in agreement with our results. Also, as explained by Fasoli *et al.* (27), Ga^{3+} doping prevents the trapping of free carriers due to shallow traps because it does not reduce the defect concentration, but rather causes changes in the valence and conduction bands such that the energy level of shallow defects is no longer in the forbidden gap where electrons can be trapped. Shallow traps are detrimental to the performance application of $\text{Y}_3\text{Al}_5\text{O}_{12}:\text{Ce}^{3+}$ in scintillators, but modifications of the band gap via substitution of $\text{Ga}^{3+}/\text{Gd}^{3+}$ can help suppress the effect (27).

Conclusion

In this study, we investigated the structural and optical properties of commercial $\text{Y}_3\text{Al}_5\text{O}_{12}:\text{Ce}^{3+}$ phosphor with regards to the substitution of Al^{3+} with Ga^{3+} and Y^{3+} with Gd^{3+} in the $\text{Y}_3\text{Al}_5\text{O}_{12}:\text{Ce}^{3+}$ garnet structure. It was found that the diffraction peaks shifted slightly to the lower angles for $\text{Y}_3(\text{Al,Ga})_5\text{O}_{12}:\text{Ce}^{3+}$ and higher angles for $(\text{Y,Gd})_3\text{Al}_5\text{O}_{12}:\text{Ce}^{3+}$ with reference to $\text{Y}_3\text{Al}_5\text{O}_{12}:\text{Ce}^{3+}$. This shift was attributed to ionic size differences; Gd^{3+} being larger than Y^{3+} and Ga^{3+} being larger than Al^{3+} . Replacing Y^{3+} with Gd^{3+} and Al^{3+} with Ga^{3+} caused lattice expansion/contraction that led to an increase/decrease in the crystal-field interaction of Ce^{3+} . The broad band excitation at 462 nm and emission at 578 nm for $\text{Y}_3\text{Al}_5\text{O}_{12}:\text{Ce}^{3+}$ were due to the 4f–5d electronic transition of Ce^{3+} ion. The UV absorption bands were found to be broad and peaked at approximately 457, 432 and 460 nm for $\text{Y}_3\text{Al}_5\text{O}_{12}:\text{Ce}^{3+}$, $\text{Y}_3(\text{Al,Ga})_5\text{O}_{12}:\text{Ce}^{3+}$ and $(\text{Y,Gd})_3\text{Al}_5\text{O}_{12}:\text{Ce}^{3+}$ powders, respectively. The highest TL signal was observed for $(\text{Y,Gd})_3\text{Al}_5\text{O}_{12}:\text{Ce}^{3+}$ with a peak at 87 °C, followed by $\text{Y}_3\text{Al}_5\text{O}_{12}:\text{Ce}^{3+}$ at 162 °C and $\text{Y}_3(\text{Al,Ga})_5\text{O}_{12}:\text{Ce}^{3+}$ at 74 °C, suggesting the existence of trap levels.

Acknowledgements

This research was jointly funded by the South African Research Chairs Initiative of the Department of Science and Technology, the National Research Foundation of South Africa and University of the Free State Cluster Fund.

References

- Bachmann VM. Studies on luminescence and quenching mechanisms in phosphors for light emitting diodes. PhD Thesis, Utrecht University, 1977:128.
- Li J, Li JG, Zhang Z, Wu X, Liu S, Li X, *et al.* Effective lattice stabilization of gadolinium aluminate garnet (GdAG) via Lu^{3+} doping and development of highly efficient $(\text{Gd,Lu})\text{AG}:\text{Eu}^{3+}$ red phosphors. *Sci Technol Adv Mater* 2012;13:035007.
- Kim MJ, Park JH, Lee KY, Lee S, Han G, Song HJ, *et al.* Cerium-doped yttrium aluminum garnet hollow shell phosphors synthesized via the Kirkendall effect. *Appl Mater Interface* 2014;6:1145–51.
- Marius M, Popovici EJ, Barbu-Tudoran L, Indrea E, Mesaros A. Cerium-doped yttrium aluminate-based phosphors prepared by wet-chemical synthesis route: modulation of the luminescence color by changing the host-lattice composition. *Ceram Int* 2014;40:6233–9.
- Upasani M, Butey B, Moharil SV. Luminescence studies on lanthanide ions ($\text{Gd}^{3+}, \text{Tb}^{3+}$) doped YAG:Ce phosphors by combustion synthesis. *J Appl Phys* 2014;6:28–33.
- Popovici EJ, Morar M, Indrea E. Synthesis and characterization of cerium doped yttrium–gadolinium aluminate phosphors by wet-chemical synthesis route. *J Opto Elect Adv Mater* 2011;13:617–24.
- Pan YX, Wang W, Liu GK, Skanthakumar S, Rosenberg RA, Guo XZ, *et al.* Correlation between structure variation and luminescence red shift in YAG:Ce. *J Alloy Compd* 2009;488:638–42.
- Liu SJ, Peng TJ, Song Z, Bian L, Song GB, Liu QL. Solid solubility and photoluminescence of $\text{Y}_3\text{Al}_5\text{O}_{12}:\text{Ce}^{3+}$ prepared by using $(\text{Y}_{1-x}\text{Ce}_x)_2\text{O}_3$ as precursor. *Chinese Phys B* 2014;23:048106(1–5).
- Xu Y, Ching WY. Electronic structure of yttrium aluminum garnet $\text{Y}_3\text{Al}_5\text{O}_{12}$. *Phys Rev B* 1999;59:530–5.
- Yousif A, Swart HC, Terblans JJ, Jafer RM, Kumar V, Kroon RE, *et al.* Structural and morphology analysis of annealed $\text{Y}_3(\text{Al,Ga})_5\text{O}_{12}:\text{Tb}$ thin films synthesized by pulsed laser deposition. *Appl Surf Sci* 2014;305:732–9.
- Li J, Li JG, Liu S, Li X, Sun X, Sakka Y. The development of Ce^{3+} -activated $(\text{Gd,Lu})_3\text{Al}_5\text{O}_{12}$ garnet solid solutions as efficient yellow-emitting phosphors. *Sci Technol Adv Mater* 2013;14:054201.
- Yang H, Yuan L, Zhu G, Yu A, Xu H. Luminescent properties of YAG:Ce³⁺ phosphor powders prepared by hydrothermal-homogeneous precipitation method. *Mater Lett* 2009;63:2271–3.
- Burda C, Chen X, Narayanan R, El-sayed MA. Chemistry and properties of nanocrystals of different shapes. *Chem Rev* 2005;105:1025–102.
- Murai S, Verschuuren MA, Lozano G, Pirruccio G, Koenderink AF, Rivas JG. Enhanced absorption and emission of $\text{Y}_3\text{Al}_5\text{O}_{12}:\text{Ce}^{3+}$ thin layers prepared by epoxide-catalyzed sol–gel method. *Opt Soc Am* 2012;2:1707–15.
- Chiang CC, Tsai MS, Hon MH. Preparation of cerium-activated GAG phosphor powders. *J Electrochem Soc* 2007;154:J326.
- Nazaraov M. Luminescence mechanism of highly efficient YAG and TAG. *Mold J Phys Sci* 2005;4:347–56.
- Dlamini STS, Swart HC, Terblans JJ, Ntwaeaborwa OM. The effect of different gas atmospheres on the structure, morphology and photoluminescence properties of pulsed laser deposited $\text{Y}_3(\text{Al,Ga})_5\text{O}_{12}:\text{Ce}^{3+}$ nano thin films. *Solid State Sci* 2013;23:65–71.
- Uysal SS, Ege A, Ayvacikli M, Khatab A, Ekdal E, Popovici EJ, *et al.* Luminescence characterization of cerium doped yttrium gadolinium aluminate phosphors. *Opt Mater (Amst)* 2012;34:1921–5.
- Rosendo L, Ricardo G. Band-gap energy estimation from diffuse reflectance measurements on sol–gel and commercial TiO_2 : a comparative study. *J Sol–Gel Sci Technol* 2012;61:1–7.
- Hom NL. Preparation and properties of long persistent SrAl_4O_7 phosphors activated by rare earth metal ions. PhD Thesis, Saga University, 2010:1–145.
- Ziyauddin M, Brahme N, Bisen DP, Kher RS. Optical properties of calcium aluminate phosphors. *Rec Res Sci Technol* 2012;4:95–6.
- You F, Bos AJJ, Shi Q, Huang S. Electron transfer process between Ce^{3+} donor and Yb^{3+} acceptor levels in the bandgap of $\text{Y}_3\text{Al}_5\text{O}_{12}$ (YAG). *J Phys Condens Matter* 2011;23:215502.
- Kshatri DS, Khare A, Jha P. Thermoluminescence studies of $\text{SrAl}_2\text{O}_4:\text{Eu}$ phosphors at different Dy concentrations. *Chalcogenide Lett* 2013;10:121–9.
- Wako AH, Dejene BF, Swart HC. Roles of doping ions in afterglow properties of blue $\text{CaAl}_2\text{O}_4:\text{Eu}^{2+}, \text{Nd}^{3+}$ phosphors. *Phys B Condens Matter* 2014;439:153–9.
- Boon KW. Physics of luminescence nanomaterials. PhD Thesis, University of Texas, 2010: 97.
- Nakazawa E, Murazaki Y, Saito S. Mechanism of the persistent phosphorescence in $\text{Sr}_4\text{Al}_{14}\text{O}_{25}:\text{Eu}$ and $\text{SrAl}_2\text{O}_4:\text{Eu}$ codoped with rare earth ions. *J Appl Phys* 2006;100:113113.
- Fasoli M, Vedda A, Nikl M, Jiang C, Uberuaga BP, Andersson DA, *et al.* Band-gap engineering for removing shallow traps in rare-earth $\text{Lu}_3\text{Al}_5\text{O}_{12}$ garnet scintillators using Ga^{3+} doping. *Phys Rev B* 2011;84:081102(R), 4.